

Anomalous magneto-elastic coupling in Au-doped BaFe_2As_2

S.-F. Wu,^{1,2,3,*} W.-L. Zhang,¹ L. Li,⁴ H.-B. Cao,⁵ H.-H. Kung,¹
A. S. Sefat,⁴ H. Ding,^{2,3,6} P. Richard,^{2,3,6,†} and G. Blumberg^{1,7,‡}

¹*Department of Physics and Astronomy, Rutgers University, Piscataway, NJ 08854, USA*

²*Beijing National Laboratory for Condensed Matter Physics,
and Institute of Physics, Chinese Academy of Sciences, Beijing 100190, China*

³*School of Physical Sciences, University of Chinese Academy of Sciences, Beijing 100190, China*

⁴*Materials Science & Technology Division, Oak Ridge National Laboratory, Oak Ridge, TN 37831*

⁵*Neutron Scattering Division, Oak Ridge National Laboratory, Oak Ridge, TN 37831*

⁶*Collaborative Innovation Center of Quantum Matter, Beijing, China*

⁷*National Institute of Chemical Physics and Biophysics, 12618 Tallinn, Estonia*

(Dated: December 7, 2017)

We used polarization-resolved Raman scattering to study magneto-elastic coupling in $\text{Ba}(\text{Fe}_{1-x}\text{Au}_x)_2\text{As}_2$ crystals as a function of light Au-doping, materials for which temperatures of the structural transition (T_S) and of the magnetic ordering transition (T_N) split. We study the appearance of the $A_g(\text{As})$ phonon intensity in the XY scattering geometry that is very weak just below T_S , but for which the intensity is significantly enhanced below T_N . In addition, the $A_g(\text{As})$ phonon shows an asymmetric line shape below T_N and an anomalous linewidth broadening upon Au-doping in the magnetic phase. We demonstrate that the anomalous behavior of the $A_g(\text{As})$ phonon mode in the XY scattering geometry can be consistently described by a Fano model involving the $A_g(\text{As})$ phonon mode interacting with the B_{2g} symmetry-like magnetic continuum in which the magneto-elastic coupling constant is proportional to the magnetic order parameter.

I. INTRODUCTION

It is widely accepted that the magnetic and electronic properties of the Fe-based superconductors are very sensitive to the As height with respect to the Fe plane, and to the Fe-As-Fe bond angle of the Fe-As tetrahedra [1–13]. The c -axis vibration of the As atom corresponds to a fully symmetric phonon mode (A_{1g}) that modulates these two parameters. First-principles calculations show that the phonon mode frequencies agree well with experiments when the Fe magnetic ordering is included [14–20], and theoretical investigations suggest that the electron-phonon coupling constant is enhanced in the magnetic state [16, 21–24]. The peak position of the fully symmetric As phonon density-of-states in the calculation with the collinear magnetic structure decreases by 23% compared with non-magnetic calculations [14]. Experimental results suggest that the fully symmetric As mode plays a major role in the electron-phonon coupling in BaFe_2As_2 [25].

Supported by previous Raman scattering investigations [26–31], recently we reported a Raman study of a variety of parent compounds of Fe-based superconductors in which we note a significant intensity enhancement, below the Néel temperature T_N , of the emergent fully symmetric As phonon mode measured in the unfavorable XY scattering geometry [32] (Fig. 1). This enhancement is found only for magnetically-ordered compounds. The results are interpreted in terms of a magneto-elastic

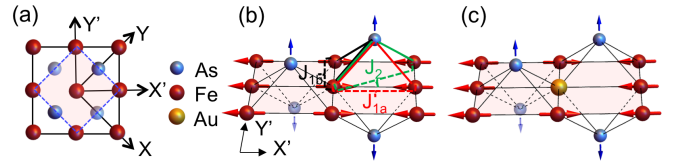


FIG. 1. (a) Definition of the X , Y , X' and Y' directions in tetragonal 2-Fe unit cell above T_S (red shaded area) and orthorhombic 4-Fe magnetic unit cell below T_N (black solid lines). (b) Schematic diagram of the magnetic ordering and of the fully symmetric As phonon mode. The red arrows mark Fe magnetic moments the collinear antiferromagnetic phase. The blue arrows indicate the As c -axes displacement. The red and black solid lines illustrate the super-exchange integrals of the nearest Fe neighbors, J_{1a} and J_{1b} . The blue solid lines illustrate the super-exchange integral of the next-nearest Fe neighbors, J_2 . (c) Illustration of disorder effect by a non-magnetic Au in the Fe plane of $\text{Ba}(\text{Fe}_{1-x}\text{Au}_x)_2\text{As}_2$.

coupling. In agreement with previous Raman studies on $\text{Ba}(\text{Fe}_{1-x}\text{Co}_x)_2\text{As}_2$ [28, 29], we also observed an asymmetric line-shape for the fully symmetric As mode below T_N in the same XY scattering geometry. Our results are described by a Fano model involving a coupling between the fully symmetric As mode and the B_{2g} electronic continuum, with the coupling constant proportional to the magnetic order parameter [32]. The purpose of this paper is to detail this model and to apply it to Au-doped BaFe_2As_2 , a system where the structural phase transition temperature T_S is a few Kelvin degrees higher than the magnetic phase transition temperature T_N [33, 34]. The experimental results support the previous observations, confirm the validity of the model, and gives about 1.5 meV as an estimate of the magneto-elastic coupling constant in the parent compound. Interestingly, we find

* sfwu@iphy.ac.cn

† pierre.richard.qc@gmail.com

‡ girsh@physics.rutgers.edu

an anomalous linewidth broadening upon Au-doping, essentially limited to the magnetic phase.

II. EXPERIMENT AND METHODS

Single crystals of $\text{Ba}(\text{Fe}_{1-x}\text{Au}_x)_2\text{As}_2$ ($x = 0, 0.012, 0.014$ and 0.031) were grown out of self-flux using a high-temperature solution-growth technique described in Refs. [33, 35], and the chemical compositions were determined by inductive coupled plasma analysis [33]. Neutron diffraction measurements on Au-doped samples were performed using the four-circle diffractometer HB-3A at the High Flux Isotope Reactor (HFIR) at the Oak Ridge National Laboratory to distinguish the structural and magnetic transitions. A neutron wavelength of 1.542 \AA was used from a bent perfect Si-220 monochromator [36]. The corresponding structural phase transi-

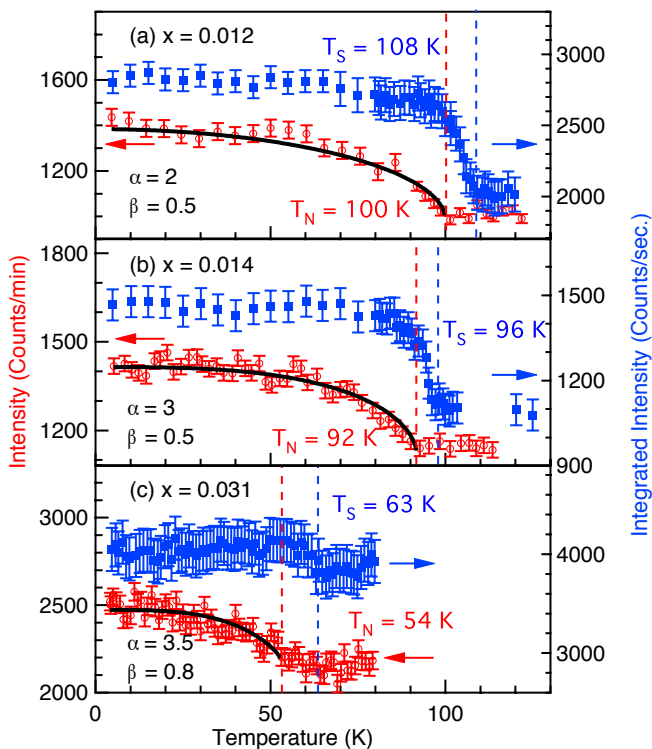


FIG. 2. Neutron diffraction results for $\text{Ba}(\text{Fe}_{1-x}\text{Au}_x)_2\text{As}_2$. (a) $x = 0.012$, (b) $x = 0.014$ and (c) $x = 0.031$. The blue solid squares represent the temperature evolution, upon cooling, of the integrated intensity of lattice Bragg peak $(2\ 2\ 0)$ in the tetragonal phase to $(4\ 0\ 0)$ in the orthorhombic phase. The red open circles represent the temperature evolution, upon cooling, of the intensity of magnetic Bragg peak $(\frac{1}{2}\ \frac{1}{2}\ 5)$ in the tetragonal phase to $(1\ 0\ 5)$ in the orthorhombic phase. The blue and red dashed lines mark T_S and T_N , respectively. The black solid curves are the fits of the temperature evolution of the intensity of magnetic Bragg peak $(1\ 0\ 5)$ with the formula $I(T) = a[1 - (T/T_N)^\alpha]^{2\beta}$.

TABLE I. Summary of the structural and magnetic phase transition temperatures (Kelvin) for samples studied in this manuscript. The last column is the ordered moment (μ_B) per Fe at 4 K determined by neutron scattering measurements.

Sample	T_S	T_N	M
BaFe_2As_2	135	135	0.87 [37]
$\text{Ba}(\text{Fe}_{0.988}\text{Au}_{0.012})_2\text{As}_2$	108	100	0.50 ± 0.02
$\text{Ba}(\text{Fe}_{0.986}\text{Au}_{0.014})_2\text{As}_2$	96	92	0.42 ± 0.04
$\text{Ba}(\text{Fe}_{0.969}\text{Au}_{0.031})_2\text{As}_2$	63	54	0.36 ± 0.02

tion temperatures (T_S) for $\text{Ba}(\text{Fe}_{1-x}\text{Au}_x)_2\text{As}_2$ are determined by the temperature evolution of the integrated intensity of lattice Bragg peak $(2\ 2\ 0)$ in the tetragonal phase to $(4\ 0\ 0)$ in the orthorhombic phase [Fig. 2]. The corresponding magnetic phase transition temperature (T_N) is determined for each sample composition from the temperature evolution of the magnetic Bragg peak intensities $(\frac{1}{2}\ \frac{1}{2}\ 5)$ in the tetragonal phase to $(1\ 0\ 5)$ in the orthorhombic phase [Fig. 2]. The T_S and T_N for the parent compound BaFe_2As_2 are determined by resistivity and magnetic susceptibility measurements [33]. All the T_S and T_N values for $\text{Ba}(\text{Fe}_{1-x}\text{Au}_x)_2\text{As}_2$ are summarized in Table I.

The crystals used for Raman scattering were cleaved and positioned in a continuous helium flow optical cryostat. The Raman measurements were performed using the Kr^+ laser line at 647.1 nm (1.92 eV) in a quasi-back scattering geometry along the crystallographic c -axis. The excitation laser beam was focused into a $50 \times 100 \mu\text{m}^2$ spot on the ab -surface, with the incident power around 10 mW . The scattered light was collected and analyzed by a triple-stage Raman spectrometer, and recorded using a liquid nitrogen-cooled charge-coupled detector.

The laser heating in the Raman experiments is determined by imaging the appearance of stripes due to twin domain formation at the structural phase transition temperature T_S [29]. When stripes appear under laser illumination, the spot temperature is just slightly below T_S , thus $T_S = kP + T_{\text{cryo}}$, where T_{cryo} is the temperature of cold helium gas in the cryostat, P is the laser power and k is the heating coefficient. By recording T_{cryo} when the stripes appear at different laser powers, we can deduce the heating coefficient using a linear fit: $k = 1 \pm 0.1 \text{ K/mW}$.

In this manuscript, we define the X and Y directions along the two-Fe unit cell basis vectors (at 45° degrees from the Fe-Fe directions) in the tetragonal phase, whereas X' and Y' are along the Fe-Fe directions [Fig. 1].

III. RESULTS AND DISCUSSIONS

The body-centered crystal structure of BaFe_2As_2 in the high temperature phase belongs to space group $I4/mmm$ (point group D_{4h}). Below T_S , the space group symmetry lowers to $Fm\bar{3}m$ (point group D_{2h}). The

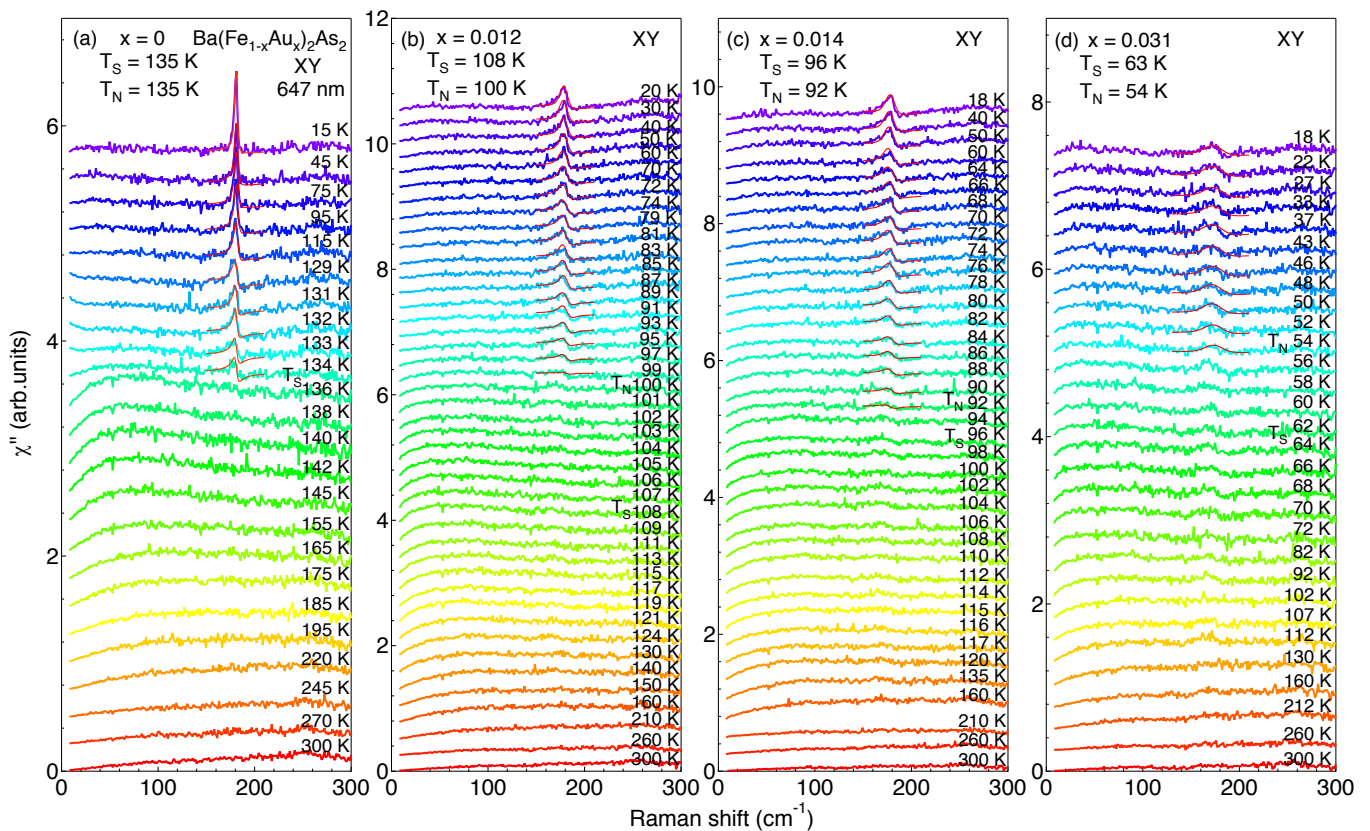


FIG. 3. T -dependence of Raman spectra in the XY scattering geometry in $\text{Ba}(\text{Fe}_{1-x}\text{Au}_x)_2\text{As}_2$. (a) $x = 0$, (b) $x = 0.012$, (c) $x = 0.014$, (d) $x = 0.031$. The solid red line are fits for the $A_g(\text{As})$ phonon mode using Eq. (3). The spectral resolution is about 0.85 cm^{-1} .

non-degenerate Raman active phonon modes at high-temperature (D_{4h}) are $A_{1g}(\text{As})+B_{1g}(\text{Fe})$. The Raman selection rules for the D_{4h} point group indicate that the XX , XY , $X'X'$ and $X'Y'$ scattering geometries probe $A_{1g} + B_{1g}$, $A_{2g} + B_{2g}$, $A_{1g} + B_{2g}$ and $A_{2g} + B_{1g}$, respectively. However, in the orthorhombic phase with D_{2h} point group symmetry, the unit cell of BaFe_2As_2 rotates by 45 degrees; the A_{1g} and B_{2g} representations of the D_{4h} point group merge into the A_g representation of the D_{2h} point group, and A_{2g} and B_{1g} (D_{4h}) merge into B_{1g} (D_{2h}).

In the orthorhombic phase, the three proper scattering

TABLE II. Summary of symmetry analysis in the D_{4h} and D_{2h} point groups [38].

Geometry	D_{4h}	D_{2h}
XX	$A_{1g}+B_{1g}$	$A_g + B_{1g}$
		not a proper geometry
XY	$A_{2g}+B_{2g}$	$A_g + B_{1g}$
		not a proper geometry
$X'X'$	$A_{1g}+B_{2g}$	A_g
$X'Y'$	$A_{2g}+B_{1g}$	B_{1g}
ZZ	A_{1g}	A_g

polarization geometries are $X'X'$, $Y'Y'$ and $X'Y'$. Since the orthorhombicity is small, the improper XX and XY polarizations still probe $A_g + B_{1g}$ and A_g symmetry excitations, respectively. The symmetry correspondence for the point groups D_{4h} and D_{2h} are summarized in Table II [39].

In Figs. 3(a)-3(d), we show detailed temperature evolution of Raman spectra for $\text{Ba}(\text{Fe}_{1-x}\text{Au}_x)_2\text{As}_2$ ($x = 0, 0.012, 0.014$ and 0.031) in the XY scattering geometry. The T_S and T_N values of each sample, carefully characterized by neutron scattering [Fig. 2], are indicated in each panel. For the parent compound BaFe_2As_2 [Fig. 3(a)], the $A_g(\text{As})$ phonon mode appears instantly below 134 K , which is close to T_S and T_N . The phonon mode rapidly sharpens upon cooling and becomes more symmetric. For $\text{Ba}(\text{Fe}_{0.988}\text{Au}_{0.012})_2\text{As}_2$, T_S (108 K) and T_N (100 K) are split. The Raman data, displayed in Fig. 3(b), show that the $A_g(\text{As})$ mode is hardly detectable between T_S and T_N . Similarly as in Co-doped BaFe_2As_2 , the mode gains strength only below T_N [40]. Although the asymmetry of the phonon line shape decreases upon cooling, we note that it remains more asymmetric than in pristine BaFe_2As_2 down to the lowest temperature. We report similar observation for $\text{Ba}(\text{Fe}_{0.986}\text{Au}_{0.014})_2\text{As}_2$ [Fig. 3(c)] and

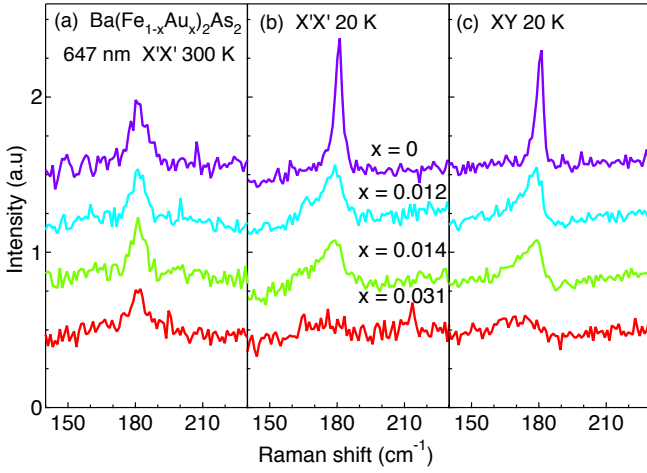


FIG. 4. (a) Doping dependence of the $A_{1g}(\text{As})$ phonon peak in $\text{Ba}(\text{Fe}_{1-x}\text{Au}_x)_2\text{As}_2$ in the $X'X'$ scattering geometry at 300 K. (b) Same as (a) but at 20 K. (c) Same as (b) but in the XY scattering geometry.

$\text{Ba}(\text{Fe}_{0.969}\text{Au}_{0.031})_2\text{As}_2$ [Fig. 3(d)] [41], although the peak becomes broader due to the disorder introduced by Au-doping.

Broadening of the spectra due to the disorder introduced from dopants is expected. However, Fig. 4 indicates that the disorder effect in $\text{Ba}(\text{Fe}_{1-x}\text{Au}_x)_2\text{As}_2$ is far from trivial. Indeed, the data show a broader line-width at 20 K than at 300 K. This should be expected only if disorder itself has a strong impact on the magneto-elastic coupling. In Figs. 4(a) and 4(b), we compare the doping evolution of the $A_{1g}/A_g(\text{As})$ phonon in the $X'X'$ scattering geometry at 300 K and 20 K. At 300 K, in the non-magnetic phase, the $A_{1g}(\text{As})$ phonon is symmetric and shows nearly doping-independent mode frequency, linewidth and intensity, as shown in Fig. 4(a). Fig. 4(b) illustrates contrasting behavior for the $A_g(\text{As})$ phonon at 20 K. We observe significant broadening, weakening, softening and a pronounced asymmetric line-shape upon Au-doping. Similar anomalous $A_g(\text{As})$ phonon behavior in the magnetic phase is also detected in the XY scattering geometry at 20 K [Fig. 4(c)].

Before moving forward with a more quantitative analysis of the $A_g(\text{As})$ phonon, it is instructive to take a closer look at the B_{1g} phonon, associated with the vibration of the Fe atom along the c axis. While below the orthorhombic transition, the A_{1g} phonon is symmetry-allowed to couple to the B_{2g} -like electronic continuum, such coupling is not possible for the $B_{1g}(\text{Fe})$ phonon, and accordingly, the line shape of this mode in the $X'Y'$ configuration remains symmetric for all temperatures. However, *a priori* the $B_{1g}(\text{Fe})$ phonon could couple to the B_{1g} -like electronic continuum. To investigate this possibility, we display in Fig. 5 the temperature evolution of the $B_{1g}(\text{Fe})$ phonon at different Au-doping levels.

Upon cooling, the $B_{1g}(\text{Fe})$ phonon mode hardens and

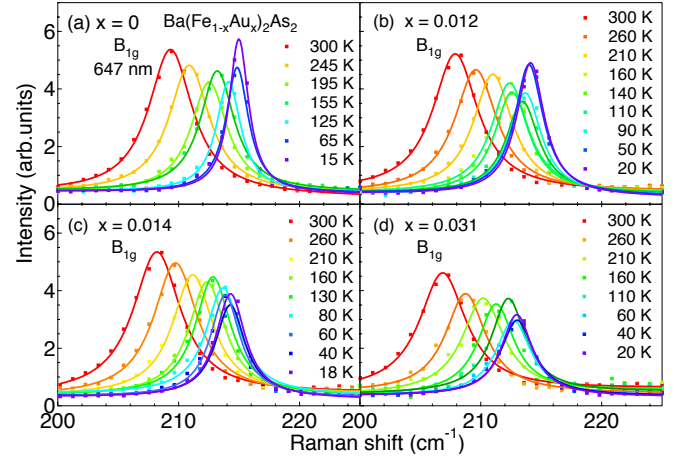


FIG. 5. T -dependence of Raman spectra of the $B_{1g}(\text{Fe})$ phonon in the $X'Y'$ geometry for $\text{Ba}(\text{Fe}_{1-x}\text{Au}_x)_2\text{As}_2$. (a) $x = 0$, (b) $x = 0.012$, (c) $x = 0.014$, (d) $x = 0.031$. The solid lines are the Lorentzian fits of the $B_{1g}(\text{Fe})$ phonon peak at different temperatures.

sharpens without detected anomalies around T_S/T_N (see Figs. 6(a)-6(d)), except for the linewidth of the parent compound BaFe_2As_2 , which displays a discontinuity around T_S/T_N [42]. The temperature dependence of the mode frequency and linewidth for the four Au-doping concentrations can be fitted by the anharmonic phonons decay model [43, 44]:

$$\omega_{ph}(T) = \omega_0 - C \left(1 + \frac{2}{e^{\frac{\hbar\omega_0}{2k_B T}} - 1} \right) \quad (1)$$

$$\Gamma_{ph}(T) = \Gamma_0 + \Gamma \left(1 + \frac{2}{e^{\frac{\hbar\omega_0}{2k_B T}} - 1} \right). \quad (2)$$

The fitting parameters are summarized in Table III. The $B_{1g}(\text{Fe})$ phonon shows slight softening and broadening upon Au doping. There is no indication of a coupling between the $B_{1g}(\text{Fe})$ phonon and the B_{1g} electronic continuum. We also note that the linewidth of the $B_{1g}(\text{Fe})$ phonon broadens only by 1 cm^{-1} from $x = 0$ to $x = 0.031$ at 20 K, demonstrating that Au-doping barely affects the $B_{1g}(\text{Fe})$ phonon, in contrast to the $A_g(\text{As})$ phonon.

As discussed in Ref. [32], the enhancement of the $A_g(\text{As})$ phonon intensity upon entering the magnetic

TABLE III. Summary of fitting parameter for $B_{1g}(\text{Fe})$ phonon mode in $\text{Ba}(\text{Fe}_{1-x}\text{Au}_x)_2\text{As}_2$.

Sample	ω_0	C	Γ_0	Γ (cm^{-1})
BaFe_2As_2	217.25	1.97	-	-
$\text{Ba}(\text{Fe}_{0.988}\text{Au}_{0.012})_2\text{As}_2$	216.54	2.02	2.14	0.67
$\text{Ba}(\text{Fe}_{0.986}\text{Au}_{0.014})_2\text{As}_2$	216.28	1.92	2.22	0.68
$\text{Ba}(\text{Fe}_{0.969}\text{Au}_{0.031})_2\text{As}_2$	215.14	1.89	2.46	0.61

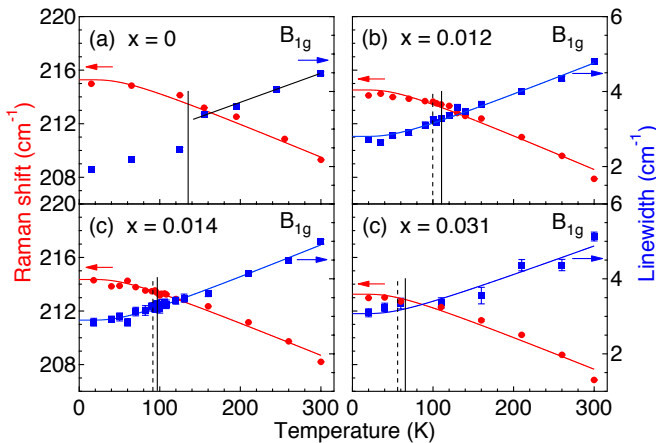


FIG. 6. T -dependence of the peak frequency (red dots) and line-width (blue squares) for the $B_{1g}(\text{Fe})$ phonon in $\text{Ba}(\text{Fe}_{1-x}\text{Au}_x)_2\text{As}_2$. (a) $x = 0$, (b) $x = 0.012$, (c) $x = 0.014$ and (d) $x = 0.031$. The solid red lines are fits for the T -dependence of the peak frequency using Eq. (1), whereas the solid blue line are fits for the T -dependence of the linewidth using Eq. (2). The vertical dashed lines represent T_N . The vertical solid black lines correspond to T_S , when different from T_N .

phase is related to the magnetic moment. Although there is increasing evidence for a description of the magnetism of the Fe-based superconductors beyond simple weak coupling or strong coupling theories [45], it worths taking a look at these theories in order to get hints on a microscopic description of the enhancement of the $A_g(\text{As})$ phonon intensity.

The enhancement of the $A_g(\text{As})$ phonon intensity can be rationalized in several ways. A previous theoretical paper [23] proposes two mechanisms to explain the enhancement of the $A_g(\text{As})$ phonon intensity due to the electron-phonon coupling upon entering the magnetic phase. The first mechanism is directly related to the geometrical parameters such as the Fe-As-Fe angle, whereas the second one has to do with the modification of the Fe-As Slater-Koster energy integrals $pd\sigma$ and $pd\pi$ due to As displacements. Both mechanisms result in finite intensity in the B_{2g} channel when the magnetic moment is finite, which is consistent with our experimental results.

The $A_g(\text{As})$ phonon intensity enhancement can also be understood from a $J_1 - J_2$ model derived from the strong coupling approach [46–48]. Here the effective nearest and next-nearest neighbors super-exchange parameters J_1 and J_2 are determined by the details of the Fe-As-Fe configuration. Below T_N , the effective super-exchange constant J_1 becomes anisotropic along the X' and Y' directions, either due to the anisotropy of the ordered magnetic moment [49], or due to the difference in the electron hopping probability along and perpendicular to the stripe directions [50]. As the $A_g(\text{As})$ phonon c -axes vibration modulates the effective super-exchange parameters J_{1a} and J_{1b} via the As bridge, $|J_{1a} - J_{1b}|$ is also modulated

because the super-exchange Fe-As-Fe path along the X' and Y' directions are different. The relative anisotropy of the in-plane electronic polarizability along the X' and Y' directions, as induced by the $A_{1g}(\text{As})$ phonon, is proportional to $|J_{1a} - J_{1b}|$. The $|J_{1a} - J_{1b}|$ term becomes nonzero only below T_N when the collinear AFM order is established, explaining why the $A_g(\text{As})$ phonon in the XY geometry appears below T_N with enhanced intensity.

Whether it originates from the local mechanism described just above, or it is caused by the bi-quadratic interaction revealed to be large due to deviations from a local picture [51], the effective $|J_{1a} - J_{1b}|$ term, proportional to the in-plane electronic polarizability, was shown to be proportional to the square of the magnetic ordered moment M [49]. Furthermore, the $A_g(\text{As})$ phonon intensity ratio in XY and XX scattering geometries I_{XY}/I_{XX} is also demonstrated to scale with the square of the magnetic ordered moment M [32]. These results suggest a magneto-elastic coupling with a strength proportional to the magnetic order parameter [25, 52, 53], a fact that we are going to exploit.

In order to quantify the electron-phonon interaction evidenced by the Raman data in the XY scattering geometry below T_N , we introduce a Fano model in which the $A_g(\text{As})$ phonon couples to the B_{2g} -like electronic continuum [32]. The resulting line shape, which describes the interference between a discrete phonon mode and an interacting continuum [54–56], has the following form:

$$I(\omega) = T_e^2 \frac{\pi \rho (\omega_0 - \omega - v \frac{T_{ph}}{T_e})^2}{(\omega_0 - \omega)^2 + (v^2 \pi \rho)^2} \quad (3)$$

where ω_0 is the bare phonon frequency, v is the magneto-elastic coupling constant, T_{ph} and T_e are the Raman coupling amplitudes to the phonon and to the electronic continuum, respectively, and ρ is the electronic density-of-states in the vicinity of the phonon frequency.

For BaFe_2As_2 , we derive the temperature dependence of the magnetic order parameter $M(T) = b(1 - T/135)^{0.103}$ obtained from the fitting of the temperature evolution of the $(1\ 0\ 3)$ magnetic Bragg peak intensity [57] (the magnetic Bragg peak intensity is proportional to the square of the magnetic order parameter). Since ω_0 barely changes upon cooling, we use the constant $\omega_0 = 181.4\text{ cm}^{-1}$ derived from the peak frequency in the XX scattering geometry at 15 K. We also fix the coupling of light to the electronic continuum $T_e^2 = 1.4$, and we keep T_{ph}/T_e and ρ as two T -dependent fitting parameters. The spectrum at 15 K is well reproduced with $T_{ph}/T_e = 0.9$, $\rho = 0.006\text{ states/cm}^{-1}$, and $v = 11\text{ cm}^{-1}$. The temperature dependence of $v(T)$, which is proportional to the magnetic order parameter, is shown in Fig. 7(a). The temperature evolutions of $T_{ph}/T_e(T)$ and $\rho(T)$ are illustrated in Figs. 7(b) and 7(c), respectively.

For Au-doped BaFe_2As_2 below T_N , we convolute the Fano intensity $I(\omega)$ with a Gaussian inhomogeneous broadening factor $\sigma(x)$. The $\sigma(x)$ broadening is determined by fitting the spectra at the lowest temperature

TABLE IV. Summary of fixed parameters.

Au-doping x	$M(T)$	$v(T)$ (cm^{-1})	ω_0 (cm^{-1})	T_e^2	$\sigma(x)$ (cm^{-1})
0	$d[1 - (T/135)]^{0.103}$	$11[1 - (T/135)]^{0.103}$	181.4	1.4	0.85
0.012	$e[1 - (T/100)]^{2 \cdot 0.25}$	$6.3[1 - (T/100)]^{2 \cdot 0.25}$	179.3	1.4	3.5
0.014	$f[1 - (T/92)]^{3 \cdot 0.25}$	$5.3[1 - (T/92)]^{3 \cdot 0.25}$	178	1.4	4.3
0.031	$g[1 - (T/53)]^{3.5 \cdot 0.4}$	$4.5[1 - (T/53)]^{3.5 \cdot 0.4}$	175	1.4	9

for each doping. The $\sigma(x)$ values are summarized in Fig. 7(d).

The temperature dependence of the (1 0 5) Bragg peak intensity below T_N is fitted with the formula $I(T) = a[1 - (T/T_N)^\alpha]^{2\beta}$, as shown in Fig. 2. Thus, the normalized magnetic order parameter $M(T)$ is obtained using $M(T) = c[1 - (T/T_N)^\alpha]^\beta$ [Table IV]. As shown in Figs. 3(b)-3(d), the Raman data for the Au-doped samples are well described by the model. The corresponding temperature dependence of $T_{ph}/T_e(T)$ and $\rho(T)$ for all Au dopings are given in Figs. 7(b) and 7(c), respectively. The sets of fixed parameters are given in Table IV. We note that we have normalized the parameters v and $\frac{T_{ph}}{T_e}$ to their values at 20 K. We also kept the electronic continuum transition matrix elements T_e the same for all Au-doping concentrations.

As shown in Fig. 7(b), the Raman coupling amplitude to the phonon (T_{ph}) increases upon cooling as an order parameter. This observation is reasonable because T_{ph} itself should be proportional to the lattice orthorhombicity δ .

The electronic density-of-states represented by the parameter $\rho(T)$ decreases upon cooling, which is consistent with the opening of a spin-density-wave gap [28, 39, 58, 59]. This observation provides a natural explanation for the reduction of the asymmetry in the $A_g(\text{As})$ phonon line shape upon cooling below T_N [28].

The parameter $\sigma(x)$ describes the inhomogeneous broadening effect due to the Au substitution of Fe. As shown in Fig. 1(c), the non-magnetic Au disorder introduced at the Fe position significantly perturbs the local magnetic order and weakens the Fe-Fe spin-spin correlation length. Indeed, only 3.1% Au-doping is sufficient to lower T_N from 135 K to 53 K. Each non-magnetic local Au dopant has four As neighbors and effectively changes the coupling strength between the $A_{1g}(\text{As})$ mode and the local Fe magnetic order parameter. The Au-doping has a major effect on the $A_g(\text{As})$ phonon, unlike the $B_{1g}(\text{Fe})$ phonon. The broadening of the $A_g(\text{As})$ phonon at $x = 0.031$ is 9 cm^{-1} , while it is only 1 cm^{-1} at 20 K for the $B_{1g}(\text{Fe})$ phonon. The significant broadening of the $A_g(\text{As})$ phonon mode upon Au-doping in the magnetic state indicates a strong coupling of the $A_g(\text{As})$ phonon to magnetism [23].

Finally, the enhanced electron-phonon coupling in the collinear AFM phase may have implications to superconductivity in the Fe-based superconductors. Earlier calculations of the electron-phonon coupling constant λ in the nonmagnetic phase led to $\lambda = 0.2$ [60]. According to

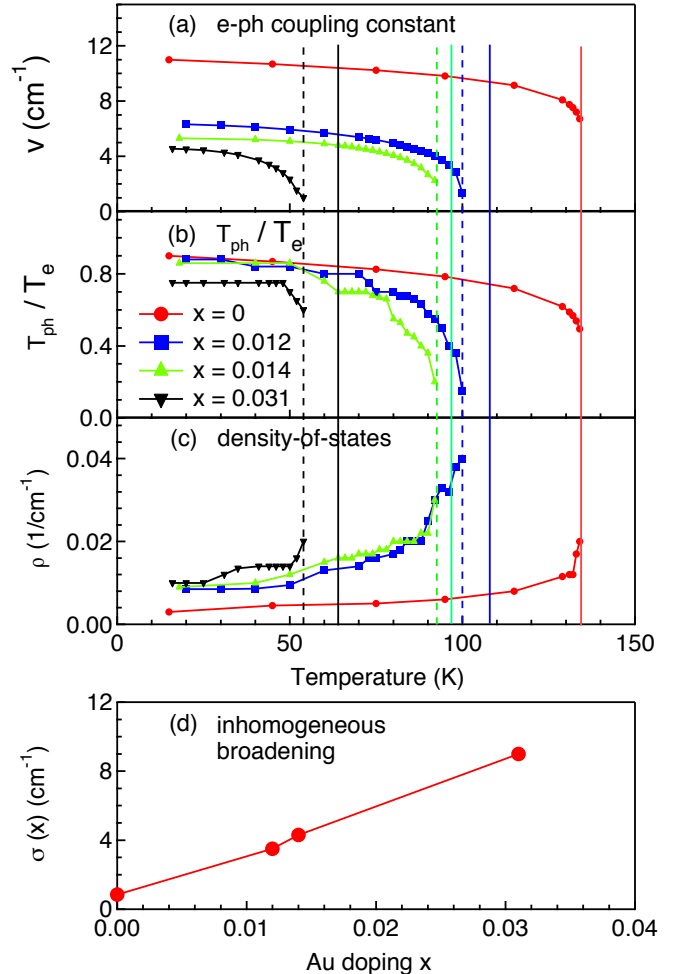


FIG. 7. T -dependence of the fitting parameters. (a) Electron-phonon coupling constant $v(T)$. (b) Ratio $T_{ph}/T_e(T)$ of the phonon transition matrix element and the electronic continuum transition matrix element. (c) Electronic density-of-states $\rho(T)$. (d) Inhomogeneous broadening factor $\sigma(x)$. $\sigma(0)$ is due to instrumental resolution. The solid lines and the dashed lines mark the corresponding T_S and T_N for the four dopings, respectively.

recent calculations, the electron-phonon matrix element is enhanced four times in the collinear AFM phase due to the presence of d_{xz}/d_{yz} Fermi surfaces around the M point [24, 61]. The enhancement is notably important at 22 meV in the Eliashberg α^2F spectral function, which coincides with the energy of the A_{1g} mode. Therefore,

the intra-band paring temperature is possibly enhanced due to the electron-phonon coupling.

IV. CONCLUSION

In conclusion, we used polarized Raman scattering to study Au-doped BaFe_2As_2 samples for which the T_S and T_N transition temperatures split. Our results confirm that the intensity of the $A_g(\text{As})$ mode in the XY scattering geometry is enhanced only below T_N and also reveal an asymmetric phonon line shape of the $A_g(\text{As})$ mode that becomes more symmetric upon cooling. To describe the line shape of the phonon peaks, we adopted a Fano model accounting for the magneto-elastic coupling. The enhancement of intensity below T_N is consistent with a magneto-elastic coupling constant proportional to the magnetic order parameter, allowing to transfer the apparent phononic Raman intensity from the electronic continuum [62]. The magneto-elastic coupling constant, estimated to about 1.5 meV in the parent compound, is non-negligible. The temperature dependence of the line shape asymmetry is explained by the interference of the coherent light scattering amplitudes due to the As phonon mode and the interacting XY -symmetry continuum, the intensity of which monotonically diminishes upon cooling as the spin-density-wave gap opens when the magnetic order develops.

We also note that when the magnetic Fe atom is substituted by non-magnetic Au at a few per cent level, the

$B_{1g}(\text{Fe})$ phonon associated with the Fe c -axis vibration shows only little disorder-induced broadening. In contrast, the anomalous A_g symmetry As mode appearing in the XY scattering geometry below T_N shows significant enhancement of the inhomogeneous broadening with Au-doping, underlying the magneto-elastic coupling mechanism. The inferred inhomogeneous broadening of the anomalous $A_g(\text{As})$ mode reaches 1 meV at 3.1% gold substitution.

The pronounced Fano line-shape and significant broadening of the $A_g(\text{As})$ phonon mode upon Au-doping in the magnetic state demonstrates the strong coupling of the $A_g(\text{As})$ phonon to magnetism and to the electronic continuum in the Fe-based superconductors, with possible consequences on the intra-band paring temperature.

ACKNOWLEDGMENTS

We thank E. Bascones and K. Haule for discussions. The research at Rutgers was supported by the US Department of Energy, Basic Energy Sciences, and Division of Materials Sciences and Engineering under Grant No. DE-SC0005463. The work at ORNL was supported by the US Department of Energy, Basic Energy Sciences, Materials Sciences and Engineering Division. Work at IOP was supported by grants from NSFC (11674371 and 11274362) and MOST (2015CB921301, 2016YFA0401000 and 2016YFA0300300) of China.

-
- [1] K. Kuroki, H. Usui, S. Onari, R. Arita, and H. Aoki, "Pnictogen height as a possible switch between high- T_c nodeless and low- T_c nodal pairings in the iron-based superconductors," *Phys. Rev. B* **79**, 224511 (2009).
 - [2] J. D. Lee, W. S. Yun, and S. C. Hong, "Ultrafast above-transition-temperature resurrection of spin density wave driven by coherent phonon generation in BaFe_2As_2 ," *New J. Phys.* **16**, 043010 (2014).
 - [3] V. Balédent, F. Rullier-Albenque, D. Colson, J. M. Ablett, and J.-P. Rueff, "Electronic properties of BaFe_2As_2 upon doping and pressure: The prominent role of the As p orbitals," *Phys. Rev. Lett.* **114**, 177001 (2015).
 - [4] V. Vildosola, L. Pourovskii, R. Arita, S. Biermann, and A. Georges, "Bandwidth and Fermi surface of iron oxypnictides: Covalency and sensitivity to structural changes," *Phys. Rev. B* **78**, 064518 (2008).
 - [5] M. J. Calderón, B. Valenzuela, and E. Bascones, "Tight-binding model for iron pnictides," *Phys. Rev. B* **80**, 094531 (2009).
 - [6] Z. P. Yin, S. Lebegue, M. J. Han, B. P. Neal, S. Y. Savrasov, and W. E. Pickett, "Electron-hole symmetry and magnetic coupling in antiferromagnetic LaFeAsO ," *Phys. Rev. Lett.* **101**, 047001 (2008).
 - [7] F. Yndurain, "Coupling of magnetic moments with phonons and electron-phonon interaction in $\text{LaFeAsO}_{1-x}\text{F}_x$," *EPL* **94**, 37001 (2011).
 - [8] C. de la Cruz, W. Z. Hu, S. L. Li, Q. Huang, J. W. Lynn, M. A. Green, G. F. Chen, N. L. Wang, H. A. Mook, Q. M. Si, and P. C. Dai, "Lattice distortion and magnetic quantum phase transition in $\text{CeFeAs}_{1-x}\text{P}_x\text{O}$," *Phys. Rev. Lett.* **104**, 017204 (2010).
 - [9] C. L. Zhang, L. W. Harriger, Z. P. Yin, W. C. Lv, M. Y. Wang, G. T. Tan, Y. Song, D. L. Abernathy, W. Tian, T. Egami, K. Haule, G. Kotliar, and P. C. Dai, "Effect of pnictogen height on spin waves in iron pnictides," *Phys. Rev. Lett.* **112**, 217202 (2014).
 - [10] C. H. Lee, A. Iyo, H. Eisaki, H. Kito, M. T. Fernandez-Diaz, T. Ito, K. Kihou, H. Matsuhata, M. Braden, and K. Yamada, "Effect of structural parameters on superconductivity in fluorine-free LnFeAsO_{1-y} ($\text{Ln} = \text{La}, \text{Nd}$)," *J. Phys. Soc. Jpn.* **77**, 083704 (2008).
 - [11] J. Zhao, Q. Huang, C. de la Cruz, S. L. Li, J. W. Lynn, Y. Chen, M. A. Green, G. F. Chen, G. Li, Z. Li, J. L. Luo, N. L. Wang, and P. C. Dai, "Structural and magnetic phase diagram of $\text{CeFeAsO}_{1-x}\text{F}_x$ and its relation to high-temperature superconductivity," *Nature Mater.* **7**, 953–959 (2008).
 - [12] K. Kuroki, H. Usui, S. Onari, R. Arita, and H. Aoki, "Pnictogen height as a possible switch between high- T_c nodeless and low- T_c nodal pairings in the iron-based superconductors," *Phys. Rev. B* **79**, 224511 (2009).
 - [13] G. Garbarino, R. Weht, A. Sow, C. Lacroix, A. Sulpice, M. Mezouar, X. Zhu, F. Han, H. H. Wen, and M. Nez-

- Regueiro, “Direct observation of the influence of the FeAs₄ tetrahedron on superconductivity and antiferromagnetic correlations in Sr₂VO₃FeAs,” *EPL* **96**, 57002 (2011).
- [14] T. Yildirim, “Frustrated magnetic interactions, giant magnetoelastic coupling, and magnetic phonons in iron pnictides,” *Physica C* **469**, 425 (2009).
- [15] L. Boeri, M. Calandra, I. I. Mazin, O. V. Dolgov, and F. Mauri, “Effects of magnetism and doping on the electron-phonon coupling in BaFe₂As₂,” *Phys. Rev. B* **82**, 020506 (2010).
- [16] M. Zbiri, H. Schober, M. R. Johnson, S. Rols, R. Mittal, Y. X. Su, M. Rotter, and D. Johrendt, “*ab initio* lattice dynamics simulations and inelastic neutron scattering spectra for studying phonons in BaFe₂As₂: Effect of structural phase transition, structural relaxation, and magnetic ordering,” *Phys. Rev. B* **79**, 064511 (2009).
- [17] D. Reznik, K. Lokshin, D. C. Mitchell, D. Parshall, W. Dmowski, D. Lamago, R. Heid, K.-P. Bohnen, A. S. Sefat, M. A. McGuire, B. C. Sales, D. G. Mandrus, A. Subedi, D. J. Singh, A. Alatas, M. H. Upton, A. H. Said, A. Cunsolo, Yu. Shvyd’ko, and T. Egami, “Phonons in doped and undoped BaFe₂As₂ investigated by inelastic x-ray scattering,” *Phys. Rev. B* **80**, 214534 (2009).
- [18] S. E. Hahn, Y. Lee, N. Ni, P. C. Canfield, A. I. Goldman, R. J. McQueeney, B. N. Harmon, A. Alatas, B. M. Leu, E. E. Alp, D. Y. Chung, I. S. Todorov, and M. G. Kanatzidis, “Influence of magnetism on phonons in CaFe₂As₂ as seen via inelastic x-ray scattering,” *Phys. Rev. B* **79**, 220511 (2009).
- [19] R. Mittal, M. K. Gupta, S. L. Chaplot, M. Zbiri, S. Rols, H. Schober, Y. Su, Th. Brueckel, and T. Wolf, “Spin-phonon coupling in K_{0.8}Fe_{1.6}Se₂ and KFe₂Se₂: Inelastic neutron scattering and *ab initio* phonon calculations,” *Phys. Rev. B* **87**, 184502 (2013).
- [20] S. E. Hahn, G. S. Tucker, J.-Q. Yan, A. H. Said, B. M. Leu, R. W. McCallum, E. E. Alp, T. A. Lograsso, R. J. McQueeney, and B. N. Harmon, “Magnetism-dependent phonon anomaly in LaFeAsO observed via inelastic x-ray scattering,” *Phys. Rev. B* **87**, 104518 (2013).
- [21] F. Yndurain and J. M. Soler, “Anomalous electron-phonon interaction in doped LaFeAsO: First-principles calculations,” *Phys. Rev. B* **79**, 134506 (2009).
- [22] G. Q. Huang, Z. W. Xing, and D. Y. Xing, “Spin-phonon coupling and effect of pressure in the superconductor LiFeAs: Lattice dynamics from first-principles calculations,” *Phys. Rev. B* **82**, 014511 (2010).
- [23] N. A. García-Martínez, B. Valenzuela, S. Ciuchi, E. Cappelluti, M. J. Calderón, and E. Bascones, “Coupling of the As A_{1g} phonon to magnetism in iron pnictides,” *Phys. Rev. B* **88**, 165106 (2013).
- [24] S. Coh, M. L. Cohen, and S. G. Louie, “Antiferromagnetism enables electron-phonon coupling in iron-based superconductors,” *Phys. Rev. B* **94**, 104505 (2016).
- [25] L. Rettig, S. O. Mariager, A. Ferrer, S. Grübel, J. A. Johnson, J. Rittmann, T. Wolf, S. L. Johnson, G. Ingold, P. Beaud, and U. Staub, “Ultrafast structural dynamics of the Fe-pnictide parent compound BaFe₂As₂,” *Phys. Rev. Lett.* **114**, 067402 (2015).
- [26] K. Y. Choi, D. Wulferding, P. Lemmens, N. Ni, S. L. Bud’ko, and P. C. Canfield, “Lattice and electronic anomalies of CaFe₂As₂ studied by Raman spectroscopy,” *Phys. Rev. B* **78**, 212503 (2008).
- [27] W. L. Zhang, P. Richard, H. Ding, A. S. Sefat, J. Gillett, S. E. Sebastian, M. Khodas, and G. Blumberg, “On the origin of the electronic anisotropy in iron pnictide superconductors,” [arXiv:1410.6452](https://arxiv.org/abs/1410.6452) (2014).
- [28] L. Chauvière, Y. Gallais, M. Cazayous, M. A. Méasson, A. Sacuto, D. Colson, and A. Forget, “Raman scattering study of spin-density-wave order and electron-phonon coupling in Ba(Fe_{1-x}Co_x)₂As₂,” *Phys. Rev. B* **84**, 104508 (2011).
- [29] F. Kretzschmar, T. Böhm, U. Karahasanovic, B. Muschler, A. Baum, D. Jost, J. Schmalian, S. Caprara, M. Grilli, C. Di Castro, J. G. Analytis, J.-H. Chu, I. R. Fisher, and R. Hackl, “Critical spin fluctuations and the origin of nematic order in Ba(Fe_{1-x}Co_x)₂As₂,” *Nat. Phys.* **12**, 560 (2016), letter.
- [30] U. F. Kaneko, P. F. Gomes, A. F. Garcia-Flores, J. Q. Yan, T. A. Lograsso, G. E. Barberis, D. Vaknin, and E. Granado, “Nematic fluctuations and phase transitions in LaFeAsO: a Raman scattering study,” [arXiv:1702.03774](https://arxiv.org/abs/1702.03774) (2017).
- [31] V. Gnezdilov, Y. G. Pashkevich, P. Lemmens, D. Wulferding, T. Shevtsova, A. Gusev, D. Chareev, and A. Vasiliev, “Interplay between lattice and spin states degree of freedom in the FeSe superconductor: Dynamic spin state instabilities,” *Phys. Rev. B* **87**, 144508 (2013).
- [32] S.-F. Wu, W.-L. Zhang, V. K. Thorsmølle, G. F. Chen, A. S. Sefat, Y. G. Shi, H. Ding, P. Richard, and G. Blumberg, “Magneto-elastic coupling in Fe-based superconductors,” Submitted to PRL.
- [33] L. Li, H. B. Cao, M. A. McGuire, J. S. Kim, G. R. Stewart, and A. S. Sefat, “Role of magnetism in superconductivity of BaFe₂As₂: Study of 5d Au-doped crystals,” *Phys. Rev. B* **92**, 094504 (2015).
- [34] S.-F. Wu, W.-L. Zhang, L. Li, H.-H. Kung, A. S. Sefat, H. Ding, P. Richard and G. Blumberg, “On the origin of critical nematic fluctuations in Fe-based superconductors,” In preparation.
- [35] A. S. Sefat, “Bulk synthesis of iron-based superconductors,” *Curr. Opin. Solid State Mater. Sci.* **17**, 59 (2013).
- [36] B. C. Chakoumakos, H. B. Cao, F. Ye, A. D. Stoica, M. Popovici, M. Sundaram, W. D. Zhou, J. S. Hicks, G. W. Lynn, and R. A. Riedel, “Four-circle single-crystal neutron diffractometer at the high flux isotope reactor,” *J. Appl. Cryst.* **44**, 655 (2011).
- [37] P. C. Dai, “Antiferromagnetic order and spin dynamics in iron-based superconductors,” *Rev. Mod. Phys.* **87**, 855 (2015).
- [38] M. Cardona and G. Güntherodt, Eds., “Light scattering in solids II, Basic Concepts and Instrumentation,” *Topics in Applied Physics* **50** (1982).
- [39] W.-L. Zhang, Z. P. Yin, A. Ignatov, Z. Bukowski, Janusz Karpinski, Athena S. Sefat, H. Ding, P. Richard, and G. Blumberg, “Raman scattering study of spin-density-wave-induced anisotropic electronic properties in AFe₂As₂ (A=Ca, Eu),” *Phys. Rev. B* **93**, 205106 (2016).
- [40] F. Kretzschmar, T. Böhm, U. Karahasanović, B. Muschler, A. Baum, D. Jost, J. Schmalian, S. Caprara, M. Grilli, C. Di Castro, J. G. Analytis, J.-H. Chu, I. R. Fisher and R. Hackl, *Nat. Phys.* **12**, 560 (2016).
- [41] We note that for Ba(Fe_{0.969}Au_{0.031})₂As₂ A_{1g}(As) phonon intensity appears above *T_S* in forbidden XY polarization (see Fig. 3(d)). The leakage is due to the local symmetry breakdown for crystals with high Au impurity concentration for which the selection rules are relaxed.

- [42] L. Chauvière, Y. Gallais, M. Cazayous, M. A. Méasson, A. Sacuto, D. Colson, and A. Forget, “Raman scattering study of spin-density-wave order and electron-phonon coupling in $\text{Ba}(\text{Fe}_{1-x}\text{Co}_x)_2\text{As}_2$,” *Phys. Rev. B* **84**, 104508 (2011).
- [43] P. G. Klemens, “Anharmonic decay of optical phonons,” *Phys. Rev.* **148**, 845 (1966).
- [44] J. Menéndez and M. Cardona, “Temperature dependence of the first-order Raman scattering by phonons in Si, Ge, and α -Sn: Anharmonic effects,” *Phys. Rev. B* **29**, 2051 (1984).
- [45] E. Bascones, B. Velazuela and M. J. Calderón, “Magnetic interactions in iron superconductors: A review,” *C. R. Physique* **36**, 17 (2016).
- [46] Q. Si and E. Abrahams, “Strong Correlations and Magnetic Frustration in the High T_c Iron Pnictides,” *Phys. Rev. Lett.* **101**, 076401 (2008).
- [47] C. Fang, H. Yao, W.-F. Tsai, J. P. Hu and S. A. Kivelson, “Theory of electron nematic order in LaFeAsO ,” *Phys. Rev. B* **77**, 224509 (2008).
- [48] C. K. Xu, M. Müller, and S. Sachdev, “Ising and spin orders in iron-based superconductors,” *Phys. Rev. B* **78**, 020501(R) (2008).
- [49] A. H. Nevidomskyy, “Interplay of orbital and spin ordering in the iron pnictides,” [arXiv:1104.1747](https://arxiv.org/abs/1104.1747) (2011).
- [50] P. W. Anderson, “New approach to the theory of superexchange interactions,” *Phys. Rev.* **115**, 2 (1959).
- [51] A. L. Wysocki, K. D. Belashchenko and V. P. Antropov, “Consistent model of magnetism in ferropnictides,” *Nat. Phys.* **7**, 485 (2011).
- [52] M. J. Han, Q. Yin, W. E. Pickett, and S. Y. Savrasov, “Anisotropy, itineracy, and magnetic frustration in high- T_c iron pnictides,” *Phys. Rev. Lett.* **102**, 107003 (2009).
- [53] S. Mandal, R. E. Cohen, and K. Haule, “Strong pressure-dependent electron-phonon coupling in FeSe,” *Phys. Rev. B* **89**, 220502 (2014).
- [54] U. Fano, “Effects of configuration interaction on intensities and phase shifts,” *Phys. Rev.* **124**, 1866 (1961).
- [55] K. Cardona, “Light scattering in solids I, Introductory Concepts,” *Topics in Applied Physics* **8** (1983).
- [56] G. Blumberg, M. V. Klein, L. Börjesson, R. Liang, and W. N. Hardy, “Investigation of the temperature dependence of electron and phonon raman scattering in single crystal $\text{YBa}_2\text{Cu}_3\text{O}_{6.952}$,” *J. Supercond* **7**, 445 (1994).
- [57] S. D. Wilson, Z. Yamani, C. R. Rotundu, B. Freelon, E. Bourret-Courchesne, and R. J. Birgeneau, “Neutron diffraction study of the magnetic and structural phase transitions in BaFe_2As_2 ,” *Phys. Rev. B* **79**, 184519 (2009).
- [58] W. Z. Hu, J. Dong, G. Li, Z. Li, P. Zheng, G. F. Chen, J. L. Luo, and N. L. Wang, “Origin of the spin density wave instability in AFe_2As_2 (A=Ba,Sr) as revealed by optical spectroscopy,” *Phys. Rev. Lett.* **101**, 257005 (2008).
- [59] P. Richard, K. Nakayama, T. Sato, M. Neupane, Y.-M. Xu, J. H. Bowen, G. F. Chen, J. L. Luo, N. L. Wang, X. Dai, Z. Fang, H. Ding and T. Takahashi, “Observation of Dirac Cone Electronic Dispersion in BaFe_2As_2 ,” *Phys. Rev. Lett.* **104**, 137001 (2010).
- [60] L. Boeri, O. V. Dolgov, and A. A. Golubov, “Is $\text{LaFeAsO}_{1-x}\text{F}_x$ an electron-phonon superconductor?” *Phys. Rev. Lett.* **101**, 026403 (2008).
- [61] S. Coh, M. L. Cohen, and S. G. Louie, “Large electron-phonon interactions from FeSe phonons in a monolayer,” *New J. Phys.* **17**, 073027 (2015).
- [62] M. V. Klein and S. B. Dierker, “Theory of Raman scattering in superconductors,” *Phys. Rev. B* **29**, 4976–4991 (1984).